

Temperature Distributions within Zeolite Precursor Solutions in the Presence of Microwaves

Murad Gharibeh,[†] Geoffrey Tompsett,[†] Fan Lu,[‡] Scott M. Auerbach,^{†,§} K. Sigfrid Yngvesson,[‡] and W. C. Conner*,[†]

Department of Chemical Engineering, 159 Goessmann Laboratory, University of Massachusetts—Amherst, Amherst, Massachusetts 01003, Department of Chemistry, 104 Lederle Graduate Research Tower, University of Massachusetts—Amherst, Amherst, Massachusetts 01003, and Department of Electrical and Computer Engineering, 201 Marcus Hall, University of Massachusetts—Amherst, Amherst, Massachusetts 01003

Received: January 14, 2009; Revised Manuscript Received: March 5, 2009

While microwave enhancement of chemical syntheses has been demonstrated for a broad variety of chemical reactions, there is no accepted universal mechanism. Is the enhancement due to more efficient heating, to overheating, to nonuniform heating, or to nonthermal effects? Analyses are complicated due to the often significant spatial and temporal temperature variations in microwave reactor systems, particularly within microwave ovens. To address this, we employ multiple fiber-optic temperature probes throughout a cylindrical reactor with a focus on zeolite synthesis solutions being the dielectric medium. First, we vary the modes of power delivery (pulsed versus continuous) to quantify differences in local temperatures within a reaction vessel with water being the dielectric medium. The temperature distribution at steady state in the center of the water increased by 10 °C in pulsed delivery mode compared to the temperature distribution obtained in continuous delivery mode at the same average power. Then, we measured the temperature distributions for several zeolite synthesis solutions (NaY, silicalite, and SAPO-11) and water under microwave heating to investigate the temperature variations within these dielectric media. These measured temperature variations were found to be significant, depending on the dielectric permittivities of the reaction medium and their changes with temperature. Temperature profiles also depend on the microwave delivery mode and reactor configuration, i.e., the microwave reactor engineering. NaY synthesis solution exhibited the smallest penetration depth (2.6 mm at room temperature and 2.45 GHz); as a result, the solution temperature near the wall increased by 65 °C over the target temperature when the temperature at the center of the solution was targeted to 60 °C. To demonstrate the effect of overheating on zeolite synthesis, we synthesized NaY zeolite at 95 °C by controlling the temperature of the reaction near the wall, close to the penetration depth, and in the center away from the penetration depth. Controlling the center temperature results in greater overheating and consequently reduced nucleation time by 80 min, from 130 to 50 min.

1. Introduction

1.1. Microwave Heating of Homogeneous vs Heterogeneous Reactions. Research into microwave (MW) chemistry has expanded over the last two decades due to the enhanced reaction rates achieved for many processes, including organic synthesis,^{1,2} inorganic synthesis,^{3–5} and polymerization;^{6,7} with over an order of magnitude time savings for many reactions, there is a great potential for energy savings⁸ and rapid processing, including continuous processing.^{9–11}

Rapid microwave heating is not solely and/or clearly proven to be the main factor contributing to the enhancement of zeolite syntheses by microwaves.^{12–14} Nevertheless, temperature distribution or temperature gradients within the heated media may occur resulting in “hot spots”. The severity of such temperature gradients depends on the dielectric properties and thus the penetration depth of the heated medium. This temperature distribution may contribute to the rate enhancement, since the rate is exponentially dependent on the temperature. For example,

Conner et al.¹⁵ found greater enhancement of silicalite synthesis in a 33 mm diameter reactor compared to an 11 mm reactor, possibly caused by nonuniformity of the MW field, which in turn depends on the dielectric properties. Indeed, the field distribution was determined using a commercial package for electromagnetic field simulation (Agilent, HFSS-software) and was shown to vary greatly depending on the vessel and hence the solution geometry.¹⁵ Furthermore, temperature variations due to macroscopic “hot spots” and/or microscopic molecular energy variations due to the “excess dipolar energy” are a possible mechanism for the rate enhancement.^{12,16}

Recently, Herrero et al.¹⁷ studied the nonthermal effects of microwave heating using multiple fiber-optic temperature probes in a reaction vessel heated by microwaves. These researchers studied four organic synthetic transformations: Diels–Alder cycloaddition, alkylation of triphenylphosphine, nucleophilic substitution of benzyl chloride with triphenylphosphine, and direct amide bond formation with both microwave heating and conventional heating. It was found that inefficient agitation leads to temperature gradients within the reaction mixture due to field inhomogeneities in the microwave cavity. Thermal gradients of 40–70 °C were reported between the probe at the top and bottom of the heated liquid, using a CEM Discover microwave

* Corresponding author. E-mail: wconner@ecs.umass.edu. Fax: +1-413-545-1647.

[†] Department of Chemical Engineering.

[‡] Department of Electrical and Computer Engineering.

[§] Department of Chemistry.

oven at 50 W. By using sufficient stirring, no differences in conversion and selectivity were observed between experiments using microwave heating and an oil bath. No evidence of nonthermal microwave effects was observed for these reactions; it was thus concluded that these effects are purely thermal. However, they studied only organic reactions in homogeneous media in a vessel size of about 10 mm, which is relatively small compared to the penetration depth of the media. Inorganic reactions with aqueous solvent, such as zeolite synthesis, typically show much higher dielectric permittivities due to the presence of polarizable dipoles. Furthermore, solid syntheses are inherently heterogeneous reactions whose interfaces can be more susceptible to microwave interactions.¹² Therefore, it is important to study the thermal gradients of these reactions, particularly in sufficiently large diameter reactors to investigate the overheating at the periphery.¹⁸

The temperature variations that may occur in zeolite precursor solutions due to the small penetration depth cannot be solely responsible for the microwave synthesis enhancement. Some zeolite precursor solutions, such as that used to synthesize SAPO-11, with relatively small dielectric permittivities and hence relatively large penetration depth (~11 mm at room temperature and 2.45 GHz) exhibit remarkable rate enhancements with the synthesis carried out in a 33 mm vessel.¹³ Temperature gradients cannot explain the rate enhancement for this synthesis, especially considering the fact that stirring the solution does not significantly affect either the nucleation or crystallization rates.¹³

Bond et al.¹⁹ showed that during microwave heating of liquids, substantial localized superheating occurs, and thus, part of the sample solution is slightly above the boiling point. The extent of superheating is of the order of several degrees.

Herrmann et al.¹⁸ measured the temperature inside a zeolite synthesis reactor vessel during microwave heating at two points, near the wall and in the center for three different zeolite precursor solutions: MFI, VFI, and LTA. These solutions have small penetration depths of 1–4 mm at 2.45 GHz. The temperature near the wall increased by about 45 °C over the set point temperature of 80 °C at the center for these solutions. The temperature variations were less pronounced in these solutions when the temperature near the wall was controlled. However, these workers did not test the hypothesis that overheating can lead to zeolite synthesis enhancement, except that previously the same group showed that a uniform field distribution led to less enhancement for NaA, NaX, VPI-5, and ZSM-5 zeolites.²⁰

1.2. Temperature Measurements during Microwave Heating. Temperature measurements within a microwave heated material are a critical concern in microwave synthesis. In previous studies, a single temperature measurement is typically reported, and sometimes none. Many of the reported rate enhancements that have been attributed to nonthermal effects may arise from thermal gradients and inaccurate temperature measurements.^{17,21,22} More careful temperature measurements are needed to explore this possibility.

The temperature of solid or liquid materials heated in a microwave field is typically measured using a fiber-optic temperature probe placed in intimate contact with the sample.²³ However, many techniques have been used to determine the temperature *in situ* during microwave heating, namely,

- (1) fiber-optic temperature probes^{23–25}
- (2) infrared thermography^{24,26,27}
- (3) gas thermometer²⁸
- (4) pyrometry^{29–31}

(5) fluorescent-coated glass^{32,33}

(6) MRI (magnetic resonance imaging) mapping^{34,35}

(7) dopant ion diffusion in ceramic sintering²⁹

(8) ad/desorption measurements³⁶

Traditional metallic thermocouples and resistance thermometry can interfere with the microwave field and may cause arcing.²⁴ However, they can and are used on several commercial microwave oven systems, e.g., Lambda Technologies Inc., Milestone, and older CEM Corp models. With grounding to prevent arcing, temperature measurements can be made this way; however, the local E-field may still be affected.

A fiber-optic temperature probe typically consists of a phosphor sensor at the end of a fiber-optic cable. The cable is sheathed in a protective coating, usually Teflon (PTFE). The phosphor emits light with temperature-dependent intensity. The light propagates down the fiber-optic cable and is measured to calculate the temperature. Fiber-optic probes provide a convenient and reliable method of measuring temperatures in a microwave field up to the temperature limit of the probe (~260 °C). However, these probes only measure the bulk (averaged) temperature at a single point and do not tell the user anything about the temperature uniformity or heating selectivity.

As mentioned above, other techniques have been employed to measure the temperature of a microwave heated material including infrared thermography. Infrared thermography employs infrared sensitive arrays or films to record an image of the infrared emission from an object just as in conventional visible light photography. The emission reflects the temperature of a heated object. Abtal et al.²⁶ in 1984 first used infrared thermography to study the evaporation of liquids in a microwave field. In food science, Mullin et al.²⁴ observed the nonuniformity of microwave heated foods with infrared thermography. An infrared camera was focused down a choke (a choke is a cylindrical tube of sufficient length to prevent escape/emission of microwaves) into a waveguide cavity to record the temperature profile of heated food.

However, it should be noted that, since infrared radiation can be absorbed by the heated material, IR thermography is restricted to surfaces and cannot be used to determine the temperature variations within a volume unless the material is relatively transparent to infrared light.³³ Further, infrared emissions are reflected by many materials that are transparent to visible light including glass. *In situ* measurements must then employ infrared transparent containers and windows.

1.3. Effect of Microwave Power Delivery on Temperature

Distributions. The interaction between microwaves and dielectric media results in molecular rotation due to the continuous change in the electric field directions. This molecular rotation causes the medium to heat up. As the medium heats and the temperature rises, the medium will change its dielectric permittivities. As a result, the microwave fields will experience a different penetration depth. Also, the microwave loss at a given point in the medium will either increase or decrease. In the case of water, the microwaves will, for example, penetrate further into the medium, and also give rise to less dielectric loss and thus less heating. When the microwaves are being delivered with the power being pulsed “on” or “off”, the medium will be able to partially cool down due to convection/conduction during the “off” period. As the microwaves are then again turned “on”, the absorption will initially be more effective than for a continuous power delivery. Therefore, it is expected that greater temperature distributions should occur with the pulsed delivery compared to those occurring with continuous mode at the same

average microwave power. Consequently, less power is required to control the medium temperature with the pulsed delivery mode.

Previously, we have shown that similar amounts of NaA zeolite product were formed from in situ WAXS experiments under the use of pulsed and continuous microwave power delivery while maintaining the same reaction temperature in a 5 mm diameter reactor.³⁷ Li and Yang reported that using pulsed microwave delivery on the synthesis of NaA zeolite membranes produced a spherical particle morphology, while using continuous microwave delivery produced cubic morphology.³⁸ Therefore, the microwave power delivery mode can affect the mesoscopic properties of the materials formed. Hence, it is an important parameter in zeolite microwave synthesis.

In this paper, first we will develop a simple temperature–time model and compare it to that obtained experimentally for water heated by microwaves under a fixed microwave fed power. Then, we illustrate the temperature variations inside a wide diameter (40 mm ID) Teflon vessel containing water and zeolite precursor solutions (silicalite, NaY, or SAPO-11) measured by fiber-optic probes at different heights and radial distances from the wall, being heated by microwaves. Overheating effect was investigated on NaY synthesis. We studied both static and stirred reactions to demonstrate the effect of agitation on this synthesis. We note that this was the approach that Kappe and co-workers employed¹⁷ to demonstrate the lack of a nonthermal microwave effect for homogeneous organic systems.

2. Experimental Section

2.1. Zeolite Precursor Solutions. Three zeolite synthesis solutions were used on the basis of their range of dielectric properties and thus their microwave penetration depth. We used example 16 from the original patent³⁹ to prepare SAPO-11 precursor solution. The solution consisted of a mixture of two organic structure directing agents prepared by combining an aqueous solution consisting of 11.53 g of 85 wt % orthophosphoric acid and 22.0 g of water with 6.9 g of a hydrated aluminum oxide (Catapal A, pseudoboehmite, 74.2 wt % Al₂O₃, 25.8 wt % H₂O) and stirring until homogeneous. We then added a mixture of 1.3 g of a fumed silica (92.8 wt % SiO₂, 7.2 wt % H₂O, CABOT) in 32.46 g of an aqueous solution of 40.0 wt % tetra-*n*-butylammonium hydroxide (TBAOH, Aldrich) to this mixture. This mixture was stirred until homogeneous, and then, 5.10 g of di-*n*-propylamine (Pr₂NH, Aldrich) was added with stirring until again homogeneous. The composition of the final reaction mixture in molar ratios was 1.0Pr₂NH:0.5(TBA)₂O:Al₂O₃:P₂O₅:0.4SiO₂:50H₂O.

Silicalite precursor solutions were prepared on the basis of the methods previously described.⁴⁰ Synthesis solutions were prepared by mixing 25 g of tetraethylorthosilicate (TEOS, Aldrich 98%), 26.25 g of 1 M tetrapropylammonium hydroxide (TPAOH) solution in water (Aldrich), and 48.75 g of H₂O, with stirring for 4 h at room temperature. Nalgene polypropylene bottles were used to mix and store the solutions.

NaY zeolite was synthesized from aged aluminosilicate gels. Colloidal silica, Ludox AS-40 (Dupont, 40 wt %, 7.76 g) was weighed into a Nalgene vessel. The proportion of water was weighed (11.76 g), 10 g of which was added to Ludox and stirred for 4–5 min. To this solution, sodium aluminate (Riedel-De Haen, 1.23 g) was added and continued to mix for another 4–5 min, until the sodium aluminate was dissolved. A small portion of the weighed NaOH (98%, Merck, 1.44 g) is then added followed by stirring until the portion is dissolved before adding more. Finally, the remaining water is added. The

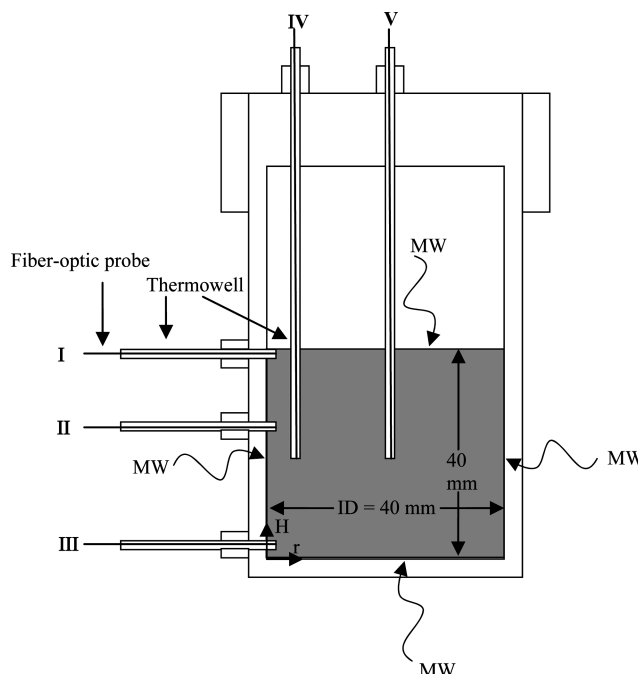


Figure 1. Schematic drawing showing the vessel constructed to measure the temperatures at different points under microwave heating.

suspension was then aged for 48 h at room temperature before reaction. The NaY precursor employed was a thick white gel with a molar composition of 8SiO₂:Al₂O₃:4Na₂O:140H₂O. Doubly distilled (DI) water was used as the pure water medium in the study.

2.2. Reaction Vessel. We have constructed a special vessel to allow us to measure the temperature at different heights (*H*) and radial distances from the wall (*r*) in a zeolite precursor solution under microwave heating (see Figure 1). Three holes were drilled in the side of the Teflon vessel (I, II, and III) at fixed heights (*H* = 38, 15, and 2 mm), respectively; in each hole, we inserted a Teflon-coated glass tube that acts as a “thermowell” to hold the fiber-optic probe. Probes IV and V were held inside sapphire tubes, “thermowells”, in the middle of the solution and at 5 and 20 mm from the wall, respectively. These tubes were held by 1/8 “Swagelok” Teflon fittings. The vessel was placed inside a 2.45 GHz CEM “MARS Xpress” microwave oven. Two types of experiments were conducted to illustrate the different heating areas inside the vessel. These experiments are

- (1) Open loop: The dielectric medium (water) was exposed to a fixed amount of microwave power and measure the temperatures using probes I, II, and III. The probes were moved closer or farther from the wall at five distances (*r* = 0, 2, 5, 10, and 20 mm) in order to measure the temperature at these points. For each temperature probe position, fresh media was used and the probe distances were set prior to heating. Probes IV and V were not used in these experiments. The power was delivered in continuous or pulsed modes. This type of experiment illustrates the interactions between the microwave radiation and the system. This enabled us to match the temperature profiles with time obtained experimentally to the heat transfer model employing our measurements of the solution dielectric properties.
- (2) Closed loop: The temperature readings by probes IV or V were controlled to a set point by varying the input microwave power via the PID controller within the

microwave oven. The other temperatures were measured and compared to the set point. Probes I, II, and III were fixed at 2 mm from the wall. This type of experiment enabled us to demonstrate temperature variations within different dielectric media (zeolite synthesis solutions and water) based on their ability to absorb microwave radiation.

2.3. Temperature Measurements. The temperatures of water heated by microwaves in the “open loop experiments” were measured by three T1 fiber-optic temperature probes by “Neoptix”, and the temperatures of the heated media in the “closed loop experiments” were measured by four T1 fiber-optic temperature probes and one provided with the microwave oven as the controlled temperature.

The “Neoptix” T1 fiber-optic temperature probes were connected to a “Neoptix–ReFlex” temperature readout which was connected to an A/D Measurement Computing USB-1208LS data acquisition board. This A/D board was interfaced with a PC computer through a USB cable. LabVIEW software by National Instruments was used to record the temperature data with time.

2.4. Microwave Ovens and Power Measurements. A CEM MARS-Xpress microwave oven was used for the “open loop experiments”. A CEM MARS-5 microwave oven was used for the “closed loop experiments”. A CEM MDS-8 ID microwave oven with in-house modification of the oven door to allow IR photography during microwave heating was used for the IR imaging experiments. The details of these ovens were previously reported.^{13,41}

The power consumed by the CEM MARS-5 microwave oven during the “closed loop experiments” was measured by a “Watts up? PRO” power meter (Electronic Educational Devices, Inc.). Stirring the precursor solution was undertaken using a magnetic stirrer bead in the solution and the CEM MARS-5 ovens built in stirrer set to “high” setting.

2.5. Infrared (IR) Imaging. IR images were taken for NaY and water samples using a ThermoVision IR camera and ThermoCAM Research pro 2.7 software both by FLIR Systems. These samples were placed in 8 oz. polystyrene cups to allow good IR transfer due to their thin polymer wall. These samples were heated in the CEM MDS-8 ID microwave oven.

2.6. Characterization. Dielectric measurements of zeolite precursor solutions were obtained using an HP 8510C Network Analyzer and HP 85070B dielectric probe (Hewlett-Packard), over a frequency range of 0.5–18 GHz. A metal short and distilled water were used to calibrate the instrument. The probe was immersed in the solution with a PTFE cap to prevent evaporation at relatively high temperatures. The temperature of the solutions was controlled by a PID controlled heating block. The dielectric data were then used to calculate the penetration depth (δ_s) as described by Tompsett et al.⁴

The crystallinity of the synthesized NaY powders was determined using X-ray diffraction. A Philips X’Pert Pro diffractometer equipped with an X’Celerator detector was used to obtain X-ray patterns. An accelerating voltage of 45 keV was used at 40 A. Patterns were obtained at a scan speed of 0.1°(2θ)/s. In order to create crystallization curves for this system, the relative peak intensity of the $hkl = 111$ and 220 peaks were ratioed against the respective peak intensities for synthesis powders at full crystallization. All X-ray patterns were matched to a standard diffraction pattern for faujasite (ICDD # 01-076-0108). The nucleation rate during zeolite synthesis was determined from the induction time prior to the crystallization of zeolites. It was estimated as the reciprocal of the induction

time necessary to achieve 1% X-ray diffraction (XRD) crystallinity.⁴² The crystallization rate was estimated from the slope of the sigmoid shaped crystallinity versus time curve between 25 and 75% relative crystallinity, where the rate is maximum.^{42–44}

The morphology and particle size of the NaY powders were determined using scanning electron microscopy (SEM). Powder samples were dispersed on aluminum stubs using an ethanol droplet followed by sputter coating with Au. A JEOL JSM-5400 scanning electron microscope was used. Particle size was determined from a statistical average of a sample population of 96 crystals from SEM micrographs using ImageJ (NIH, U.S.) software.

3. Energy Balance

In order to understand the energy transfer between microwaves and solutions, we begin with the basic energy balance. As a result, a model for the temperature profile with time can be developed. This model can then be compared to the experimental data. If the model fits the data well, the data can be interpreted by the physics of the model.

The general energy balance for a dielectric medium heated by microwaves at any fixed point in space is given by eq 1:

$$\text{Energy in} - \text{Energy out} + \text{Energy generation} = \text{Energy accumulation} \quad (1)$$

$$\text{MW}(T) - \text{UA}(T - T_o) + 0 = mC_p \frac{dT}{dt} \quad (2)$$

where

MW(T): microwave absorbed power as a function of temperature (T)

U : the overall heat transfer coefficient

A : the surface area of the system

m : the mass of the system

C_p : the specific heat capacity of the system

t : time

Assuming that the absorbed microwave energy (MW) and C_p are not strong functions of temperature, and the material does not expand significantly so that the surface area stays constant, the solution for the above ordinary differential equation with the initial condition $T(0) = T_o = 23$ °C is given as

$$T(t) = T_o + \left(\frac{\text{MW}}{\text{UA}} \right) \left[1 - \exp\left(-\left(\frac{\text{UA}}{mC_p}\right)t\right) \right] \quad (3)$$

Once the microwave power is turned off, the temperature decreases in an exponential decay. According to the solution of eq 2 obtained with disregarding the energy input term (MW) and with the initial condition $T(0) = T_{ss}$ (the steady state temperature), the cooling temperature profile is given as

$$T(t) = T_o + (T_{ss} - T_o) \exp\left(-\left(\frac{\text{UA}}{mC_p}\right)t\right) \quad (4)$$

The steady state solution is simply given by balancing the “energy in” with “energy out”, obtained by setting the accumulation term in eq 2 to zero

$$\text{MW} = \text{UA}(T_{ss} - T_o) \quad (5)$$

Figure 2 shows a typical temperature profile with time for water being heated with microwaves at any point in space and fixed microwave input power. It also illustrates the three different regions: heating, steady state, and cooling.

However, when we fitted the temperature data for microwave heated water with eqs 3 and 4, we found that the exponential term exhibited a different exponent upon heating and cooling.

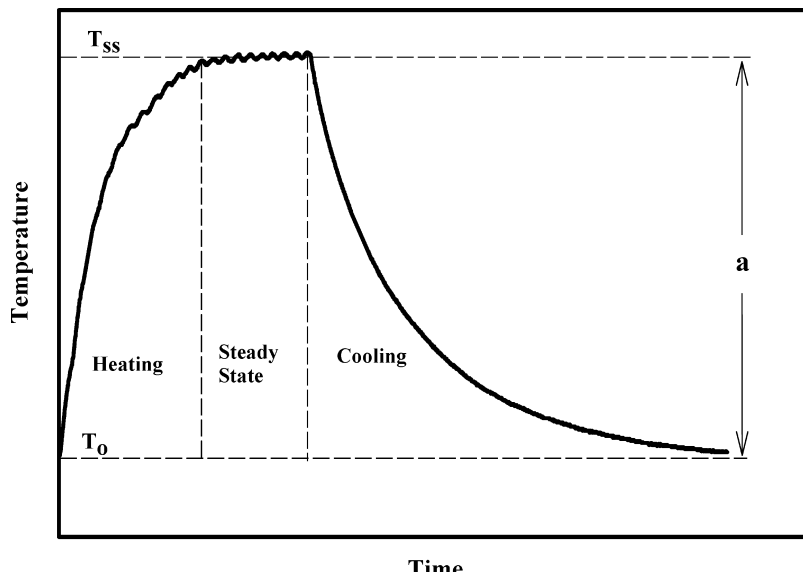


Figure 2. Typical experimental temperature profile with time at any point in space for DI water being heated by microwaves at fixed microwave fed power.

TABLE 1: Summary of the Energy Balance at Different Heating Stages

stage	energy balance
heating	$T(t) = T_0 + \frac{\alpha}{UA - \beta} \left(1 - \exp\left(-\frac{UA - \beta}{mC_p} t\right) \right)$
steady state	$\alpha + \beta(T_{ss} - T_0) = UA(T_{ss} - T_0)$
cooling	$T(t) = T_0 + (T_{ss} - T_0) \exp\left(-\left(\frac{UA}{mC_p}\right)t\right)$

That contradicts what these two equations predict, since that exponent is the same in both equations ($-(UA/mC_p)$). This indicates that the assumption that the absorbed microwave power (MW) is not a function of temperature is incorrect. We have modified the model by introducing a linear function of MW with temperature (MW = $\alpha + \beta(T - T_0)$) in eq 2. This maintains the dependency of temperature with time to be of the form $T = T_0 + a(1 - \exp(-bt))$ which the experimental data follow very well.

The new model modifies the heating equation to be

Heating:

$$T(t) = T_0 + \frac{\alpha}{UA - \beta} \left(1 - \exp\left(-\frac{UA - \beta}{mC_p} t\right) \right) \quad (6)$$

A summary of the energy balance equations is listed in Table 1.

Thus, if the mass and the heat capacity of the heated material are known, one can fit the experimental data (temperature vs time) in the heating and cooling regions to their corresponding models, shown in Table 1, to obtain the fitting parameters α , β , and UA .

On the basis of the work of Metaxas and Meredith,⁴⁵ English and MacElroy⁴⁶ have shown that for a given constant volume

of material heated by uniform electric field “ $E_{max} \cos(\omega t)$ ” the temperature dependence on time is given as

$$\omega \varepsilon_o \varepsilon''(\omega, T) E_{max}^2 \cos^2(\omega t) = \rho C_v(\rho, T) \frac{dT}{dt} \quad (7)$$

where

C_v : the constant volume heat capacity

ρ : the density of the dielectric medium

ω : the microwave field frequency

ε'' : the imaginary part of the dielectric constant which determines the dielectric loss

ε_o : the dielectric permittivity of vacuum

Assuming that C_p and C_v are approximately equal and weak functions of temperature, the volume of the heated medium is constant, and the dielectric loss is linear with temperature ($\varepsilon'' = A + B(T - T_0)$) at a given frequency, then the left-hand side of eq 7 is equal to the microwave energy input term ($\alpha + B(T - T_0)$) in eq 2 divided by the volume of the heated material (V), i.e.,

$$\omega \varepsilon_o (A + B(T - T_0)) E_{max}^2 \cos^2(\omega t) = (\alpha + \beta(T - T_0))/V \quad (8)$$

Consequently, $\alpha = \omega \varepsilon_o A E_{max}^2 \cos^2(\omega t) V$ represents the microwave power absorbed by the dielectric medium at a given temperature and $\beta = \omega \varepsilon_o B E_{max}^2 \cos^2(\omega t) V$ represents the gradient in the microwave power absorbed by the dielectric medium as its temperature changes.

Thus,

$$B/A = \beta/\alpha \quad (9)$$

Equation 9 basically indicates that a dielectric medium interacts thermally with microwaves on the basis of how its ε'' value changes with temperature. If ε'' decreases with temperature (B is negative), then that dielectric medium becomes less susceptible to microwave heating as its temperature increases and vice versa.

4. Results and Discussion

4.1. Open Loop: Temperature Distribution Using a Pure Dielectric Medium—Water.

We have measured the temperature profile of 49.3 g of DI water under a continuous microwave

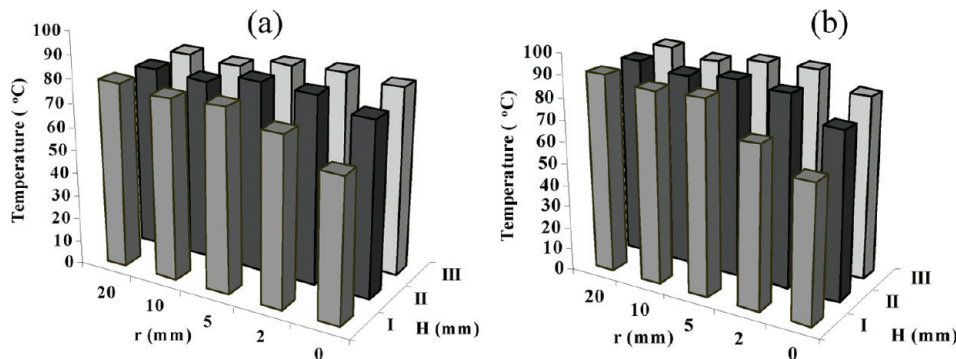


Figure 3. Steady state temperature distributions within DI water using an average power of 68 W and (a) continuous power delivery and (b) pulsed: 1 s on/2 s off. Open loop experiment.

power delivery of 68 W and with a pulsed power of 204 W (these microwave powers represent the microwave power fed by the oven) at a sequence of (1 s on/2 s off), which results in an average power of 68 W.

The temperatures were measured at three heights ($H = 2$ (III), 15 (II), and 38 (I) mm) from the bottom of the vessel and the experiments were repeated using fresh DI water and the three probes (I, II, and III) were moved to five radial distances from the wall ($r = 0, 2, 5, 10$, and 20 mm). The vessel was mounted on a turntable to average the microwave field intensity within the vessel. Thus, we assume a symmetrical temperature distribution around the center of the vessel. Figure 3 shows the steady state temperature distribution as a function of height and radial distance from the wall for continuous and pulsed delivery with an average power of 68 W.

In both delivery modes, the temperature variation is a maximum near the wall where the bottom temperature ($H = \text{III}$ and $r = 0$) is the highest and the top temperature at ($H = \text{I}$ and $r = 0$) is the lowest. This could be due to the fact that microwaves can be delivered to the bottom as well as to the top, but the thick base of the Teflon vessel minimizes the heat loss while the air in contact with the top surface maximizes the heat loss. Moreover, the temperature distributions obtained under heating with the pulsed microwave power delivery mode are overall higher than those in the continuous microwave power delivery mode. For example, the temperature in the center of the vessel is 90 °C for the pulsed microwave power delivery and 80 °C in continuous microwave power delivery.

Temperature variations decrease near the center of the vessel away from the cooler wall under microwave heating. This is likely due to good heat transfer (convection and conduction) between the bottom, center, and top. The relatively long penetration depth of microwaves in water (~ 33 mm at room temperature and 2.45 GHz) compared to the radius of the vessel (20 mm) allows microwaves to penetrate throughout the water liquid volume in the 40 mm diameter vessel. Thus, the water in the center is being heated readily by the microwaves. This produces relatively uniform temperature distributions, as seen in Figure 3.

The dielectric loss (ϵ''), dielectric permittivity (ϵ'), and penetration depth (δ_s) of water are dependent on the temperature and the frequency (see the Supporting Information). At any microwave frequency in the range of 0.5–18 GHz, both ϵ' and ϵ'' decrease as the temperature increases, leading to an increase in the penetration depth, e.g., at 4 GHz, the penetration depth increases from 12 to 55 mm when heating from 28 to 72 °C. Figure 4 shows a linear decrease in both ϵ' and ϵ'' with temperature at 2.45 GHz is a good fit to the measured data for water. This leads to an exponential increase in the penetration

depth with temperature. These results help to explain why pulsed microwave delivery heats water more than continuous microwave delivery. In particular, as the water heats up, its ability to absorb microwaves decreases because of the decrease of ϵ'' with the increase in temperature. Thus, when the power is pulsed, the “off” period allows the system to relax, and therefore, the heat is lost from the hotter regions to the colder regions, lowering the temperature of the hotter regions, which enables them to absorb more microwaves in the “on” period. This relaxation occurs to a lesser degree when the power is continuously delivered. As a result, the pulsed power delivery leads to higher temperatures inside the vessel compared to that obtained by continuous power delivery for the same average microwave fed power, as shown in Figure 3.

“SigmaPlot 2000” software by SPSS Inc. was used to fit the temperature data (temperature vs time) to obtain the dielectric parameters (α, β). Table 2 shows the average values of these parameters over all points. The dielectric loss (ϵ'') describes the ability of the material to convert the absorbed microwaves to heat. Figure 4 shows that, at 2.45 GHz, ϵ'' for water decreases linearly with temperature according to $\epsilon'' = 9.79 - 0.18(T - T_0)$. This results in B/A equal to -0.018 , where A is the intercept and B is the slope of the line. The averaged ratios of β/α were calculated at the wall ($r = 0$) at the three different heights for both continuous and pulsed schemes (Table 2). The temperatures near the wall experience heat loss mainly from the adjacent cold wall, which fits the assumption of the heat balance established in eq 2. The β/α ratio is the same order of magnitude as the B/A ratio for the continuous power delivery as eq 9 predicts. However, this ratio is an order of magnitude less than that of B/A for the pulsed power delivery. This could be due to the fact that the “off” period in the pulsed sequence enhances the heat flow and, thus, the thermal equilibration within the material. This type of heat flow was not considered in the energy balance shown in eq 2. Nonetheless, the analysis shown above captures most of the qualitative aspects of the experimental data very well.

4.2. Microwave Heating of Zeolite Precursor Solutions.

The dielectric properties of zeolite synthesis solutions are significantly different from those of pure water, due mainly to the presence of various ions in the solution. These include silicate anions and organic cations that act as structure directing agents (templates). Further, the pH of precursor solutions is either acidic or very basic, contributing to the high permittivities through high concentrations of either hydronium or hydroxide ions. The large difference in the dielectric properties between NaY and silicalite and SAPO-11 precursor solutions can be attributed to the ionic concentration of the solutions.⁴⁷ Silicalite synthesis solution is a relatively dilute solution at pH ~ 12 , and

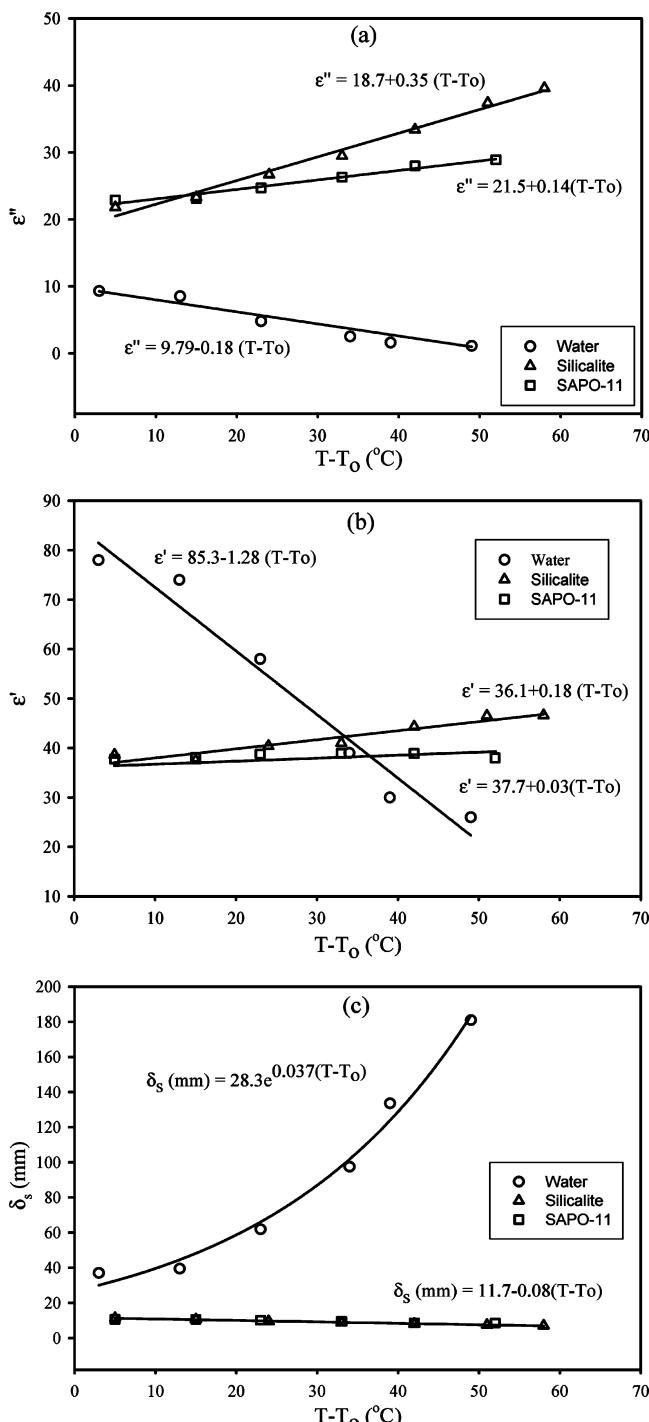


Figure 4. The dependence of the dielectric properties of water, silicalite, and SAPO-11 synthesis solutions on temperature at 2.45 GHz: (a) dielectric loss (ϵ''); (b) dielectric permittivity (ϵ'); (c) penetration depth (δ_s).

TABLE 2: The Overall Average Values of the Predicted Dielectric Parameters for Water at 2.45 GHz and the Average Ratio of These Parameters at the Wall

delivery mode	$(UA)_{\text{overall}}$ (W/K)	$(\alpha)_{\text{overall}}$ (W)	$(\beta)_{\text{overall}}$ (W/K)	$(\beta/\alpha)_{\text{at the wall}}$ (K ⁻¹)
continuous	0.16	17.7	-0.16	-0.012
pulsed (1 s on/ 2 s off)	0.16	20.2	-0.12	-0.008

SAPO-11 synthesis solution, although containing a high concentration of ions, has a more neutral pH of ~ 6 . Comparatively,

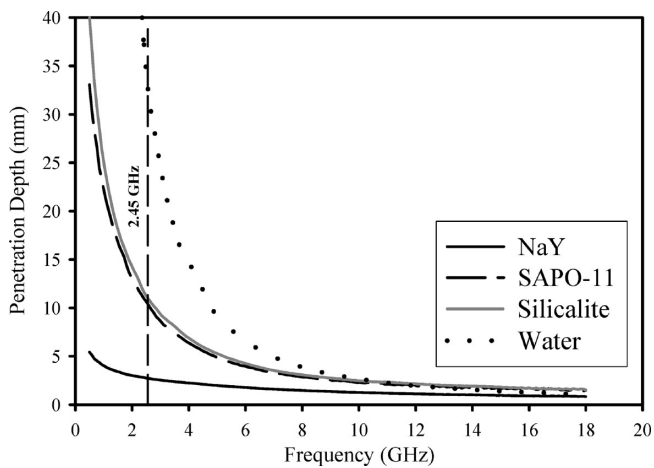


Figure 5. Penetration depth dependence on microwave frequency of zeolite precursor solutions and water at room temperature.

NaY synthesis solution contains a high concentration of ions and is at a high pH of ~ 12 .

Both ϵ' and ϵ'' increase with temperature for silicalite and SAPO-11 synthesis solutions, as shown in Figure 4. This results in a slight decrease in the penetration depth for these synthesis solutions with the increase in temperature (Figure 4). However, the dielectric properties (ϵ' and ϵ'') show a strong dependence on frequency, which results in a strong penetration depth dependence on frequency (Figure 5). The increase in ϵ'' for the synthesis solution with temperature will result in a positive value of β -positive feedback heating. This indicates that the zeolite synthesis solutions will reach higher temperatures and will heat more rapidly than water for a given volume under the same microwave fed power.

The dissipation factor ($\tan \delta$) indicates the efficiency of the dielectric medium in converting microwave energy into heat. Zeolite synthesis solutions have a higher, up to an order of magnitude, dissipation factor than water (Table 3) that makes them more susceptible to microwave heating. Furthermore, the small penetration depth of these synthesis solutions compared to water, especially at 2.45 GHz (Figure 5), indicates that the absorbed microwave energy will concentrate in a thin outer layer of these solutions when placed in a vessel with a diameter larger than their penetration depth while the absorbed microwave energy will be more or less even throughout the volume in the case of water.

To directly test this prediction, we placed 72 mL of NaY synthesis solution and the same volume of water in two identical thin walled 8 oz. polystyrene cups. Both samples were placed inside a microwave oven and heated simultaneously for 1 min under 320 W. IR images were recorded during the heating process of these two materials. Figure 6 shows these images at different times. It is clear that NaY synthesis solution heats faster and reaches higher temperatures compared to water. Further, thermal images of the top surfaces of both heated materials were recorded at the end of the heating period (Figure 7). These images show the effect of penetration depth on the thermal distribution within the dielectric media. NaY synthesis solution shows a great thermal variation (about 40 °C) between the hot region near the wall (70 °C) and the cold core (32 °C), while water shows a homogeneous thermal distribution of about 60 °C.

The next section demonstrates this difference in the thermal distribution between water and zeolite synthesis solutions and its implication on the synthesis enhancement in further detail.

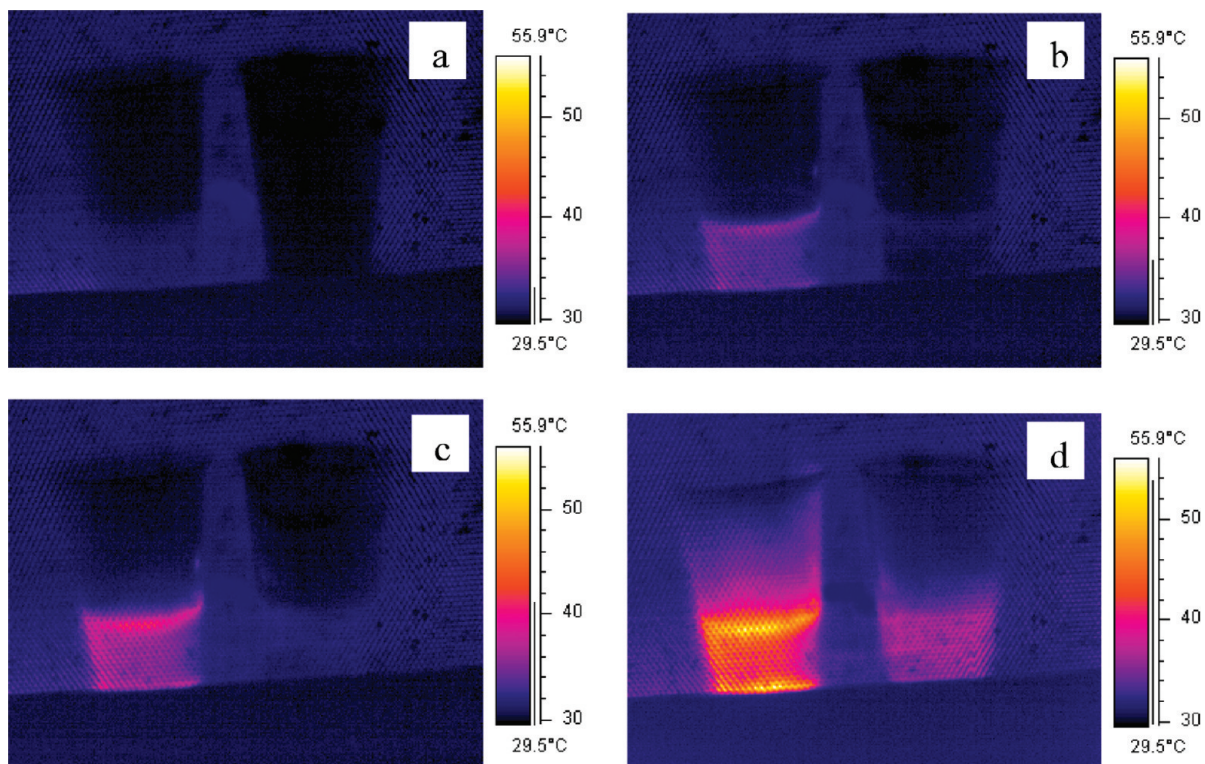


Figure 6. In situ IR images (side view) for NaY synthesis solution (left sample) and water (right sample) heated at 320 W. Images taken at (a) 0 s, (b) 10 s, (c) 20 s, and (d) 60 s.

TABLE 3: Dielectric Constants (ϵ' , ϵ''), Dissipation Factor ($\tan \delta$), and Penetration Depth (δ_s) of Zeolite Precursor Gels (2.45 GHz, Room Temperature)

medium/zeolite precursor	molar composition	density (g/mL)	pH	ϵ'	ϵ''	$\tan \delta = \epsilon''/\epsilon'$	δ_s (mm)
water ⁴	H ₂ O	1.00	7.0	78	10	0.13	33.4
silicalite	SiO ₂ :0.23TPAOH:32.88H ₂ O	0.98	12.4	49.5	20.13	0.41	13.8
SAPO-11	1.0Pr ₂ NH:0.5(TBA) ₂ O:Al ₂ O ₃ :P ₂ O ₅ :0.4SiO ₂ :50H ₂ O	1.11	6.2	37.8	22.9	0.61	10.8
NaY (AS-40)	4Na ₂ O:Al ₂ O ₃ :8SiO ₂ :140H ₂ O	1.36	12.24	37	147	3.98	2.6

4.3. Closed Loop: Temperature Distribution in Zeolite Precursor Solutions. Three zeolite precursor solutions, namely, those for silicalite, NaY, and SAPO-11, as described in the Experimental Section, were employed to determine the effect of position of temperature control and the resulting temperature distributions within the solutions. These zeolite precursor solutions were chosen due to the range of their dielectric properties and compositions.

The densities of the zeolite solutions are silicalite, 0.98 g/mL; SAPO-11, 1.11 g/mL; NaY, 1.36 g/mL. The density of the solution does play a significant role in the dielectric properties

which are dependent on the ion concentration. NaY synthesis solution has a relatively high concentration and hence higher density compared to silicalite and SAPO-11 synthesis solutions. NaY synthesis solution is similar in density (~1.2–1.3 g/mL) to the zeolite gel precursors LTA, MFI, and VFI used by Herrmann et al.¹⁸ to demonstrate the overheating effect.

Both silicalite and SAPO-11 precursor solutions have similar dielectric properties at 2.45 GHz (typical microwave oven frequency). However, the NaY precursor solution shows significantly higher dielectric loss ($\epsilon'' = 147$), and therefore will have greater coupling with the microwave field and smaller penetration depth (Table 3).

Figures 8–11 show the microwave delivered power and the temperatures measured at the five positions (I, II, III, IV, and V) using temperature control at position V (middle center of solution) set to 60 °C, for the three zeolite precursor solutions NaY, SAPO-11, and silicalite and water, respectively. A ramp time of 3 min to 60 °C was used in all cases and the temperature was held for up to 60 min to obtain steady state. This temperature is lower than the synthesis temperatures for all three materials. This prevents the synthesis solutions from significant reaction, which can change the dielectric properties dramatically. It can be seen that the NaY synthesis solution with the shortest penetration depth exhibits the greatest temperature overshoot of 13 °C between the measured controlled temperature at the center (V) and the set point of 60 °C. The temperature difference in the solution between the highest temperature near the wall

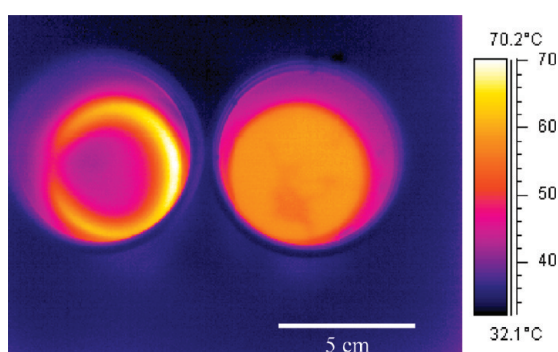


Figure 7. Ex situ IR images (top view) for NaY synthesis solution (left sample) and water (right sample) heated under 320 W at the end of the heating period.

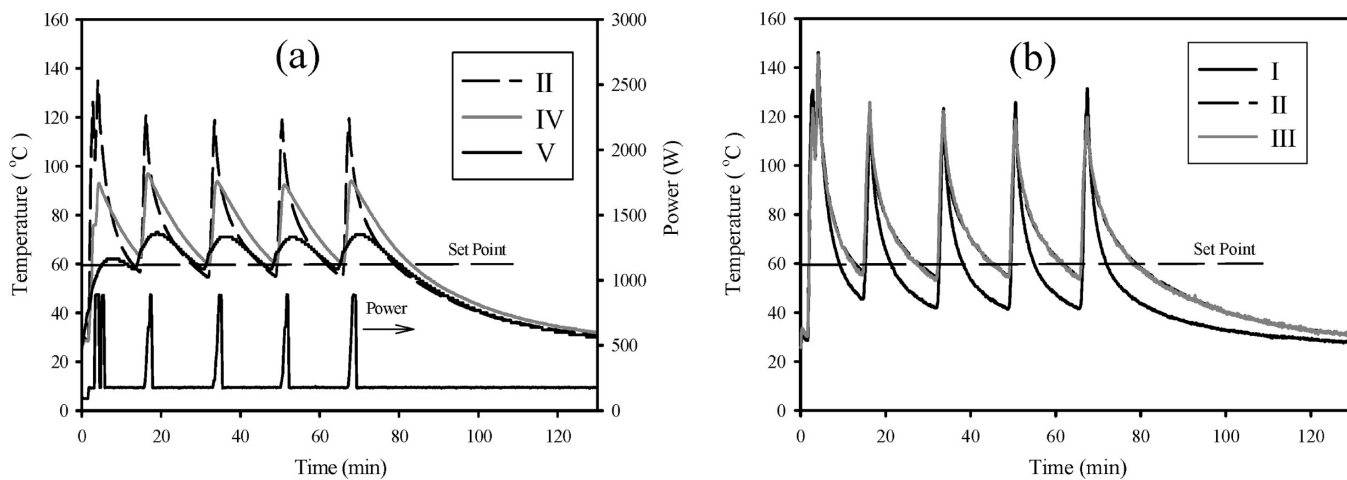


Figure 8. Microwave oven output power and temperature measured within NaY precursor solution heated at a set point of 60 °C at position V: (a) center positions; (b) wall positions. Ramp time: 3 min.

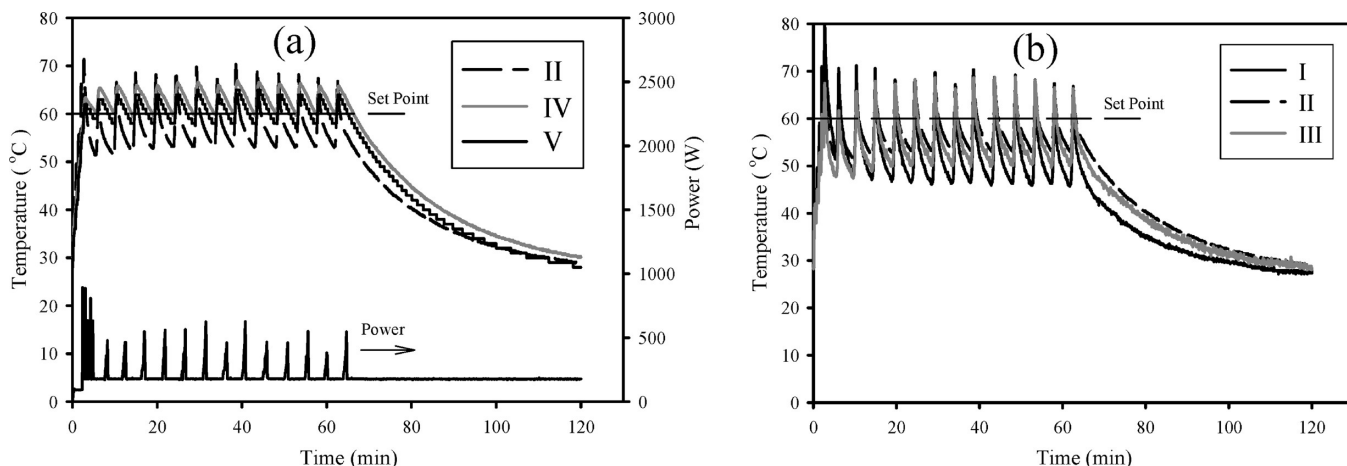


Figure 9. Microwave oven output power and temperature within SAPO-11 precursor solution heated at a set point of 60 °C at position V: (a) center positions; (b) wall positions. Ramp time: 3 min.

and the set temperature is also quite high, near 65 °C. In comparison, silicalite and SAPO-11 solutions show overshooting of only 2 and 7 °C, respectively, and a temperature difference of only ~5 and 10 °C, respectively. Further, the silicalite solution shows a lower average temperature near the vessel wall (I, II, and III) compared to the center (V). The relatively large penetration depth of microwaves in silicalite and SAPO-11 solutions compared to NaY gives rise to the solution heating from the center out rather than the microwaves primarily absorbed at the surface.

In comparison to the zeolite precursor solutions (Figures 8, 9, and 10), water overshoots by ~1 °C at the center and there is a temperature difference of ~3 °C (Figure 11). The relatively high penetration depth of water (33 mm) allows microwaves to be absorbed throughout the medium, and the lower temperatures near the wall are likely due to the heat loss through the wall to the surrounding air.

Since there is a significant (65 °C) temperature difference in the unstirred NaY solution during microwave heating to 60 °C, stirring the solution during heating is likely to decrease the gradient through mixing. Figure 12 shows the microwave power delivered and the temperatures measured at the five positions (I, II, III, IV, and V) using temperature controlled at position V (middle center of solution) with a set point of 60 °C, for NaY precursor solution with stirring. Overshooting in the solution with stirring still occurs, but by only 7 °C at the control

temperature above the 60 °C set point at the center (V). A temperature difference of 50 °C is measured compared to 65 °C for the unstirred case (Figure 8). Stirring decreases the temperature gradient in the vessel cross section. However, significant overheating is still measured at the bottom of the vessel. The stirring may not be rapid or even enough to account for the rapid microwave absorption, because the solution gels as it heats and the stirring bead and the bottom probe were at opposite sides of the vessel.

Table 4 shows the energy consumption per gram of different materials heated to 60 °C in 3 min and held at that temperature for 1 hour. The heated mass differs from one material to another because of the difference in density and because the vessel was filled to the same volume. Therefore, the volume of the samples was fixed but not the mass. From Table 4, it can be seen that the energy per gram decreases from water, silicalite, SAPO-11, to NaY precursor solutions as the dielectric loss increases and hence the penetration depth decreases (Table 3). This suggests that ionic solutions exhibit the greatest temperature spikes upon microwave heating, while dipolar liquids like water give the greatest bulk microwave heating.

The energy per gram of the stirred NaY precursor is again lower than that for static NaY solution. It requires less energy to maintain the average temperature of a stirred solution because stirring enhances the heat transfer from the hot regions near the wall to the center where the temperature is being controlled.

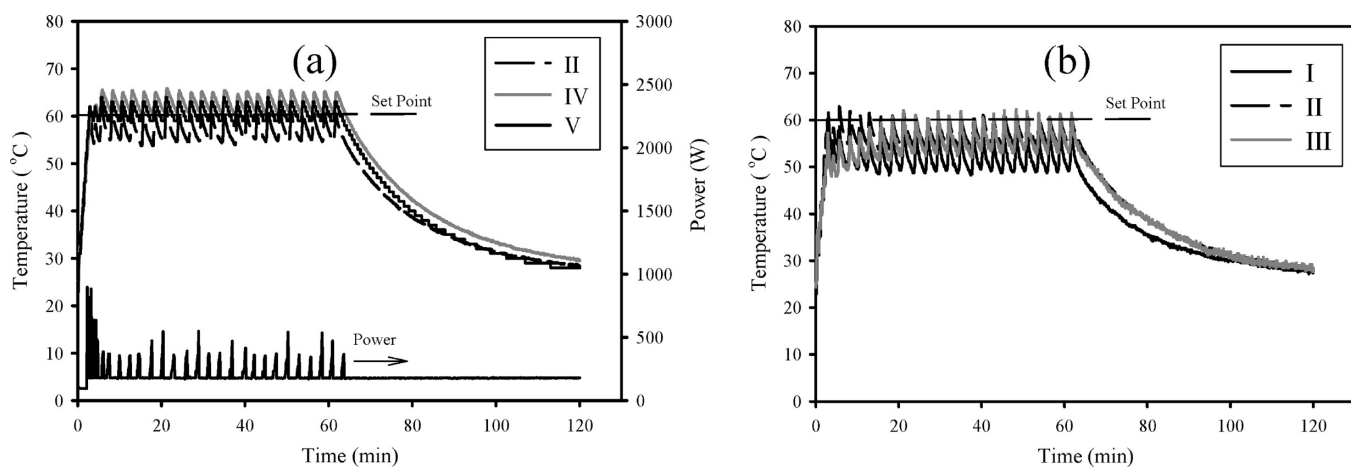


Figure 10. Microwave oven output power and temperature within silicalite precursor solution heated at a set point of 60 °C at position V: (a) center positions; (b) wall positions. Ramp time: 3 min.

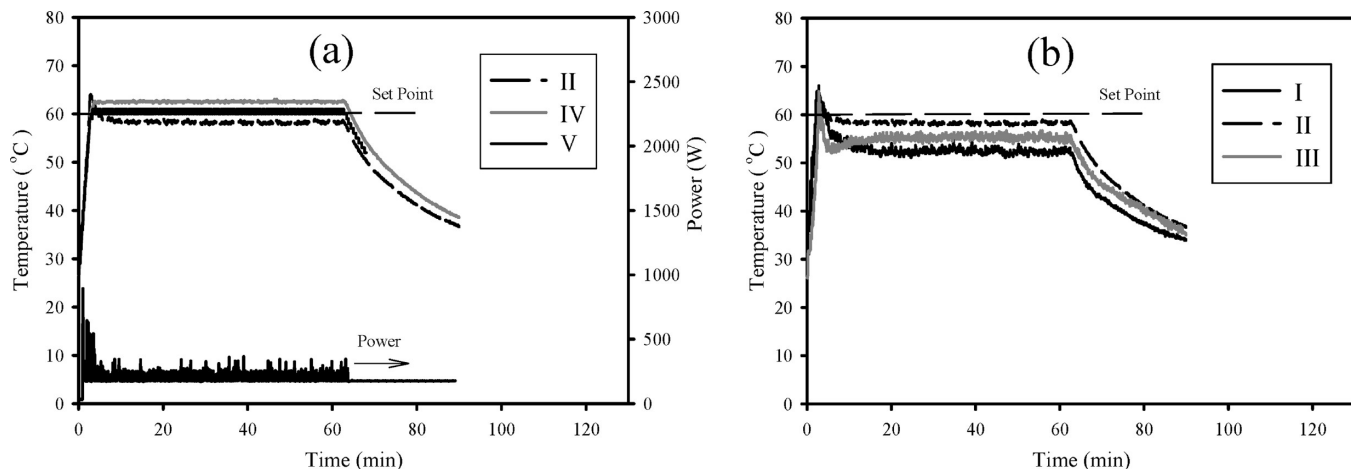


Figure 11. Microwave oven output power and temperature within water heated at a set point of 60 °C at position V: (a) center positions; (b) wall positions. Ramp time: 3 min.

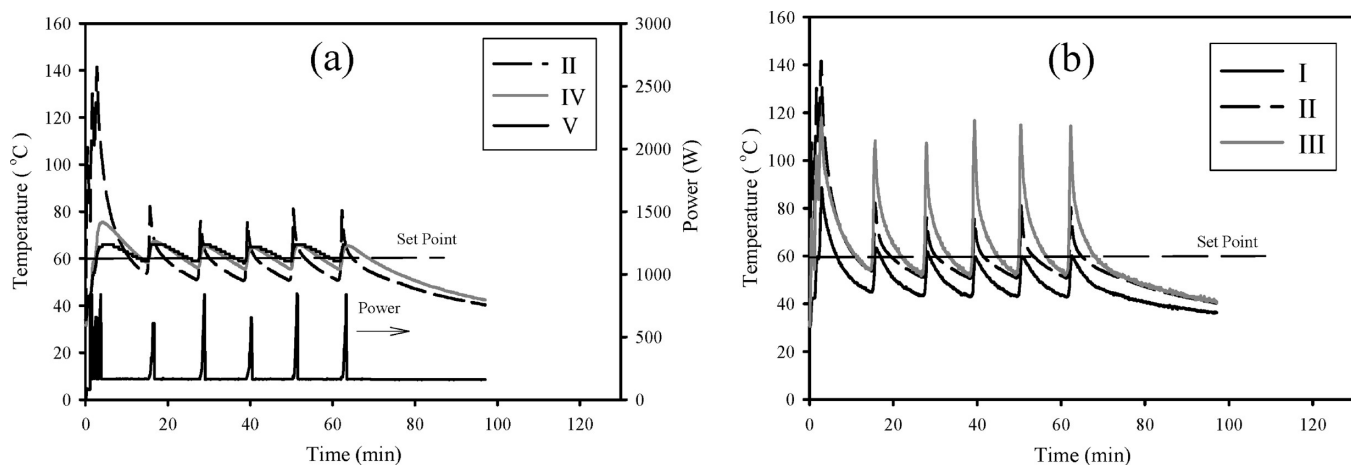


Figure 12. Microwave oven output power and temperature within stirred NaY precursor solution at a set point of 60 °C at position V: (a) center positions; (b) wall positions. Ramp time: 3 min.

A summary of the temperature differences and overheating measured in the temperature distribution experiments described above is shown in Table 5. Water, silicalite, and SAPO-11 precursors show only a small temperature difference and thus small overheating due to the relatively long penetration depth compared to the vessel diameter. The penetration depth for these media is sufficient to allow microwaves to pass throughout the vessel. Hence, no significant "skin" heating of the periphery is

observed and the lower temperature at the periphery is likely due to heat loss to the surrounding air.

NaY synthesis solution exhibits the greatest temperature differences and overheating due to the relatively small penetration depth (2.6 mm at room temperature and 2.45 GHz). Stirring the precursor solution reduced but did not eliminate the overheating (50 °C compared to 65 °C).

TABLE 4: Energy Consumption of a Fixed Volume of Zeolite Precursor Solutions (and Water) Heated to 60 °C at 3 and 60 min Hold Times (MARS-5 (CEM) Microwave Oven and Savillex PFA Vessel)

material	weight (g)	energy (Wh)	energy per gram (Wh/g)
water	49.30	225	4.56
silicalite	49.07	214	4.36
SAPO-11	55.24	208	3.76
NaY	68.20	238	3.49
NaY-stirred	68.20	197	2.88

TABLE 5: Summary of the Steady State Temperature Gradients and Overshooting for Temperature Distribution Experiments Using a 40 mm Vessel and the CEM MARS-5 Oven (Temperature Set Point 60 °C Controlled at Position V (Center), 3 min Ramp Time)

medium	stirring	temperature difference between the highest temperature and the set temperature (°C)	overshoot (difference between the measured controlled temperature and its set point) (°C)
water	N	3	1
silicalite	N	5	2
SAPO-11	N	10	7
NaY	N	65	13
NaY	Y	50	7

4.4. Effect of Overheating on NaY Synthesis. Herrmann et al.¹⁸ studied zeolite precursor solutions with short penetration depths such as LTA, MFI, and VFI in order to demonstrate the overheating at the vessel periphery. Similarly, we focused on the NaY precursor solution temperature distribution and synthesis, since this material exhibits the greatest temperature difference between the region near the wall and the center due to its relative short penetration depth of microwaves. To demonstrate the overheating effect on this zeolite synthesis, NaY zeolite was synthesized from its precursor solution under microwave heating while controlling the temperature at either the middle center (position V) or the periphery (position IV). The precursor solution was heated to 95 °C with 12 min ramp time and held at that temperature for different times. Figure 13 shows the temperature measured at position I through V in NaY synthesis solution controlled by the fiber-optic probe at position V (center). Controlling the center temperature (position V) produces a large overheating effect of up to ~50 °C at the wall and a gradient from the wall to the center of ~30 °C (between positions II and V).

When the temperature at the periphery (position IV) was controlled, the overheating effect was reduced. Figure 14 shows the temperature measured at position I through V for NaY synthesis solution heated to 95 °C controlled by the probe at position IV (periphery). Compared to the temperature profile shown in Figure 13 for center probe control, it is obvious that there is significantly less overheating effect with an overshoot of only ~2 °C and a gradient between the wall and center of 12 °C. The temperature near the vessel wall is controlled, and the center maintains a slightly lower temperature at steady state (~85 °C) due to heat transfer limitations. As a result, in order to maintain a more even temperature distribution in the microwave heated sample, controlling the periphery temperature is preferred for this system. However, it has been shown that for some zeolite syntheses nonuniform heating typically enhances the reaction rate.^{15,48}

An additional experiment was undertaken by using stirring in addition to temperature control at the center position (V) in order to create a more even temperature distribution while

controlling the temperature at the center. Figure 15 shows the temperature measured at position I through V for NaY solution heated to 95 °C controlled by the probe at position V, with simultaneous stirring of the solution. Compared to the temperature profile shown in Figure 13 for center probe control without stirring, it is obvious that there is an intermediate overheating effect with an overshoot of only ~10 °C and a difference between the wall and center of 30 °C. Indeed, stirring decreases the overheating effect but not to the extent of that produced from controlling the temperature at the periphery.

Figure 16 shows crystallization curves for NaY synthesized at 95 °C up to 6 h with 12 min ramp time. Controlling the temperature at the periphery of the vessel delays the nucleation of NaY by approximately 80 min compared to that obtained from controlling the center temperature. However, the crystallization rate is similar (0.010 compared to 0.017 min⁻¹). Controlling the temperature at the periphery (IV) causes less temperature variations to occur within the solution (Figures 12 and 13), which leads to a longer nucleation time. These findings are in complete agreement with what we reported previously on this zeolite synthesis in two reactor geometries with 11 and 33 mm diameter vessels. The bigger the vessel diameter to penetration depth ratio, the greater the chance for thermal variations. The NaY synthesis in the 33 mm diameter vessel reduced the nucleation time by 100 min compared to the 11 mm vessel, where the crystallization rates were found to be similar.⁴⁸

Furthermore, the zeolite precursor was stirred during microwave heating controlled at the center in order to demonstrate the effect of mixing on the solution and hence evening out the temperature variations during synthesis. It can be seen in Figure 16 that the crystallization curve for this control mode shifts to slower nucleation, i.e., toward that obtained with control at the periphery. Stirring thus was found to delay nucleation to 90 min compared to 50 min for center (V) controlled without stirring. However, the nucleation is not delayed to the same extent as that produced by the static solution with controlling the periphery temperature (IV).

This may indicate that the rate enhancement effect due to microwave heating is not purely an overheating effect and that, even with greater temperature uniformity on the macroscopic level in the vessel by stirring the heated solution, microscopically there is still an athermal energy distribution¹⁶ and hence a microwave effect.¹² Table 6 lists the nucleation times, crystallization rates, particle size, and numbers for the synthesis of NaY at 95 °C using temperature control at the center and periphery. Particle sizes are determined from samples at the initial maxima in the crystallization curves (the beginning of the plateau region). SEM was used to determine particle sizes; the number of particles was estimated from the average size and yield. Figure 17 shows the SEM micrographs of NaY zeolite from microwave synthesis at 95 °C using center control (V), periphery control (IV), and center control (V) with stirring. There is no significant difference in the product zeolite particle sizes among the three methods of temperature control. Therefore, the synthesis rate is predominantly dependent on the rate of nucleation and the difference in crystallization rates does not produce significant differences in particle sizes or morphology.

In order to determine if Ostwald ripening is a possible process during this synthesis of NaY under differently controlled microwave heating, the particle sizes and numbers were measured at longer times in the plateau region on the crystallization curves. The SEM micrographs of NaY samples prepared using center (V) and periphery control (IV) are shown in Figure

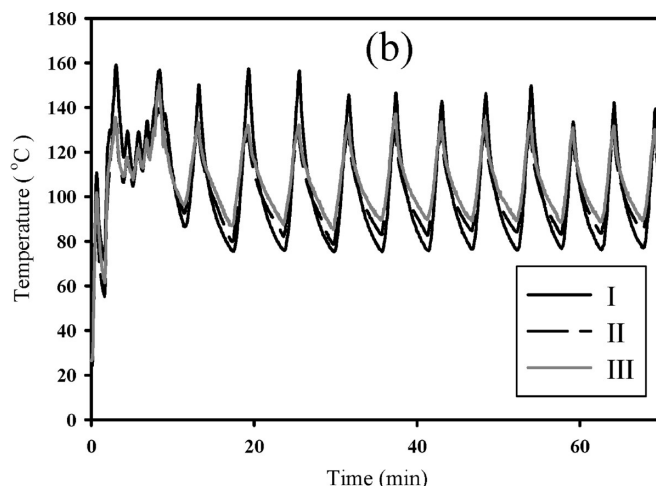
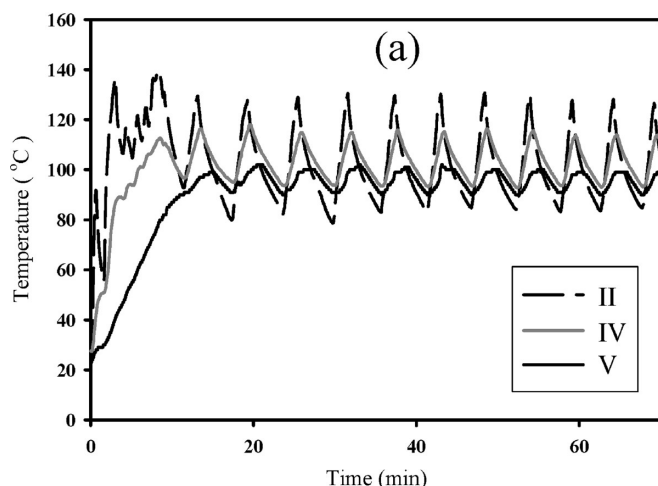


Figure 13. Temperature measured within NaY precursor solution at a set point of 95 °C at position V: (a) center positions; (b) wall positions. Ramp time: 12 min.

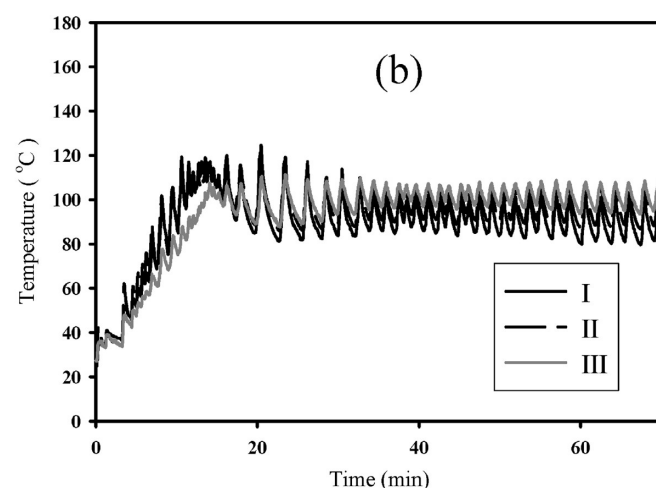
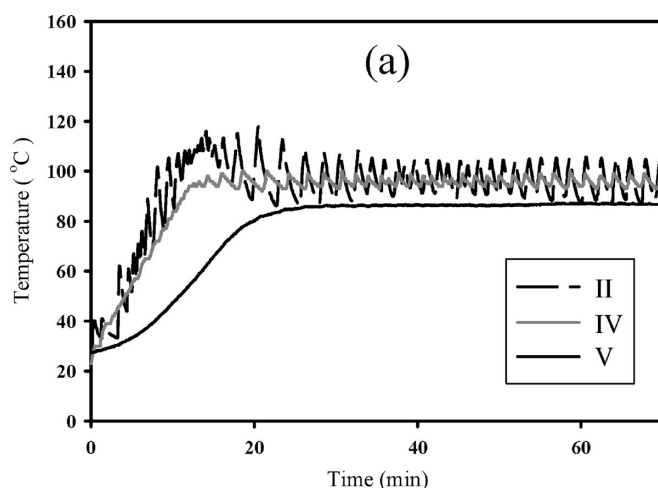


Figure 14. Temperature measured within NaY precursor solution at a set point of 95 °C at position IV: (a) center positions; (b) wall positions. Ramp time: 12 min.

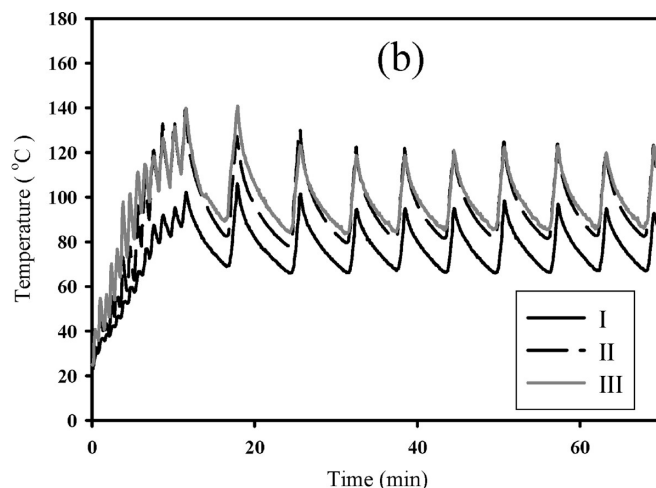
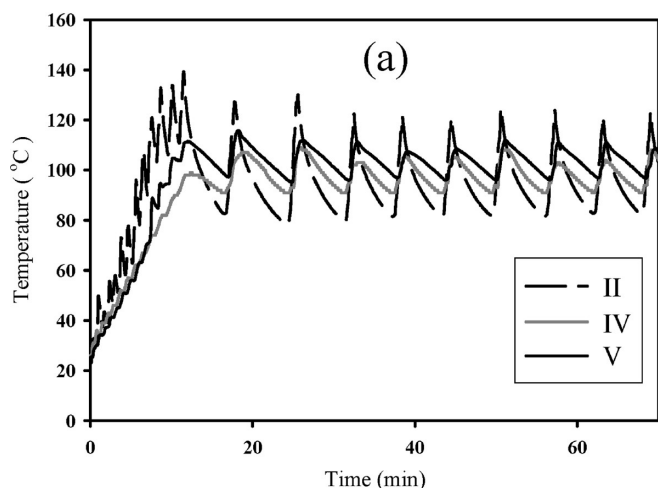


Figure 15. Temperature measured within NaY precursor solution at a set point of 95 °C at position V with stirring: (a) center positions; (b) wall positions. Ramp time: 12 min.

18. The particle morphology is similar for all samples; i.e., all particles are spherical. The measured particle sizes and estimated number of particles are shown in Table 7 for the samples at the end of the plateau region on the crystallization curves using either center (with and without stirring) or periphery temperature control. The particle sizes increased with increasing time of the

reaction. Furthermore, the estimated numbers of particles decreased with increasing reaction time. This increase in the particle sizes and decrease in the particle numbers, especially for the stirred and periphery controlled syntheses, indicates that Ostwald ripening is a possible mechanism of growth in these two cases. It is clear that with stirring the solubility of the small

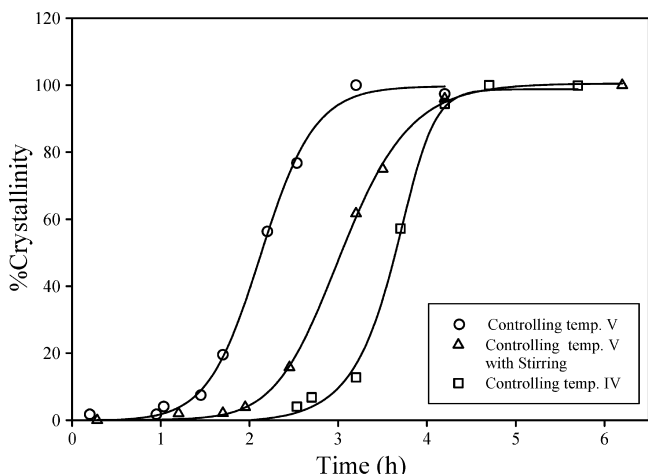


Figure 16. Crystallization curves for NaY zeolite prepared using microwave heating with the microwave power controlled by the temperature at position V without stirring, position V with stirring, and position IV without stirring all at 95 °C and 12 min ramp time.

TABLE 6: The Nucleation Times, Crystallization Rates, and Energy Consumption of NaY Zeolite Synthesis Using Temperature Control at Different Positions Within the Reactor (Particle Sizes and Numbers for the Samples at the Beginning of the Plateau Region on the Crystallization Curves)

controlled temperature	ramp time (min)	nucleation time (min)	crystallization rate (min^{-1})	energy consumption at 50% crystallization (Wh)	particle size ^a (μm)	yield (g)	estimated number of particles ^b $\times 10^{12}$
center middle (V), no stirring	12	50	0.010	650	0.38 ± 0.12	10.65	287
periphery middle (IV), no stirring	12	130	0.017	720	0.40 ± 0.08	10.17	235
center middle (V), with stirring	12	90	0.009	700	0.40 ± 0.13	10.02	231

^a Statistical size distribution based on 96 crystals. ^b Assuming spherical particles. Density⁴⁹ of 1.29 g cm^{-3} .

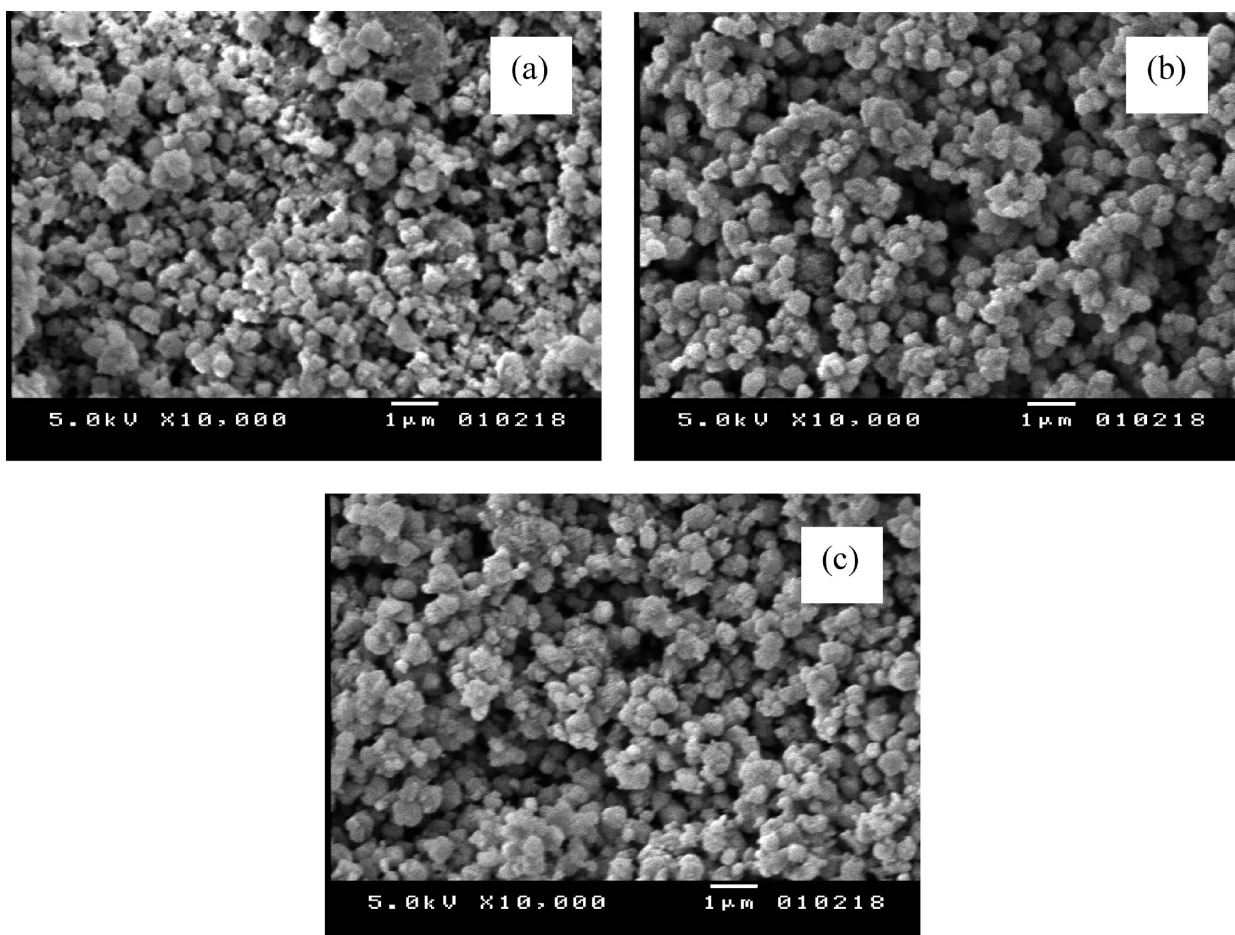


Figure 17. SEM micrographs of NaY zeolite from microwave synthesis using (a) center control (position V) without stirring, (b) periphery control (position IV) without stirring and (c) center control (position V) with stirring. For the samples at the beginning of the plateau region on the crystallization curves.

particles increases, which enhances the growth of the large particles. However, it is not clear why this mechanism will occur in the periphery control synthesis. Nevertheless, this phenomenon was observed for stirred⁵⁰ and static^{51,52} synthesis of NaA zeolite. Furthermore, it was also reported that this process is possible for other zeolite syntheses such as silicalite synthesis by both conventional and microwave heating.^{15,53,54}

5. Conclusions

We have investigated the temporal and spatial properties of microwave heating of DI water (dipolar liquid) and zeolite precursor solutions (ionic solutions) to shed light on the macroscopic distributions of energy in these systems.

Initially, distilled water was used to demonstrate the thermal processes induced by microwave heating. An energy balance was applied to the system heated by microwaves at a fixed average power of 68 W. Two delivery modes were investigated: continuous and pulsed (1 s on/2 s off). Higher temperatures were reached by pulsed power delivery compared to that by

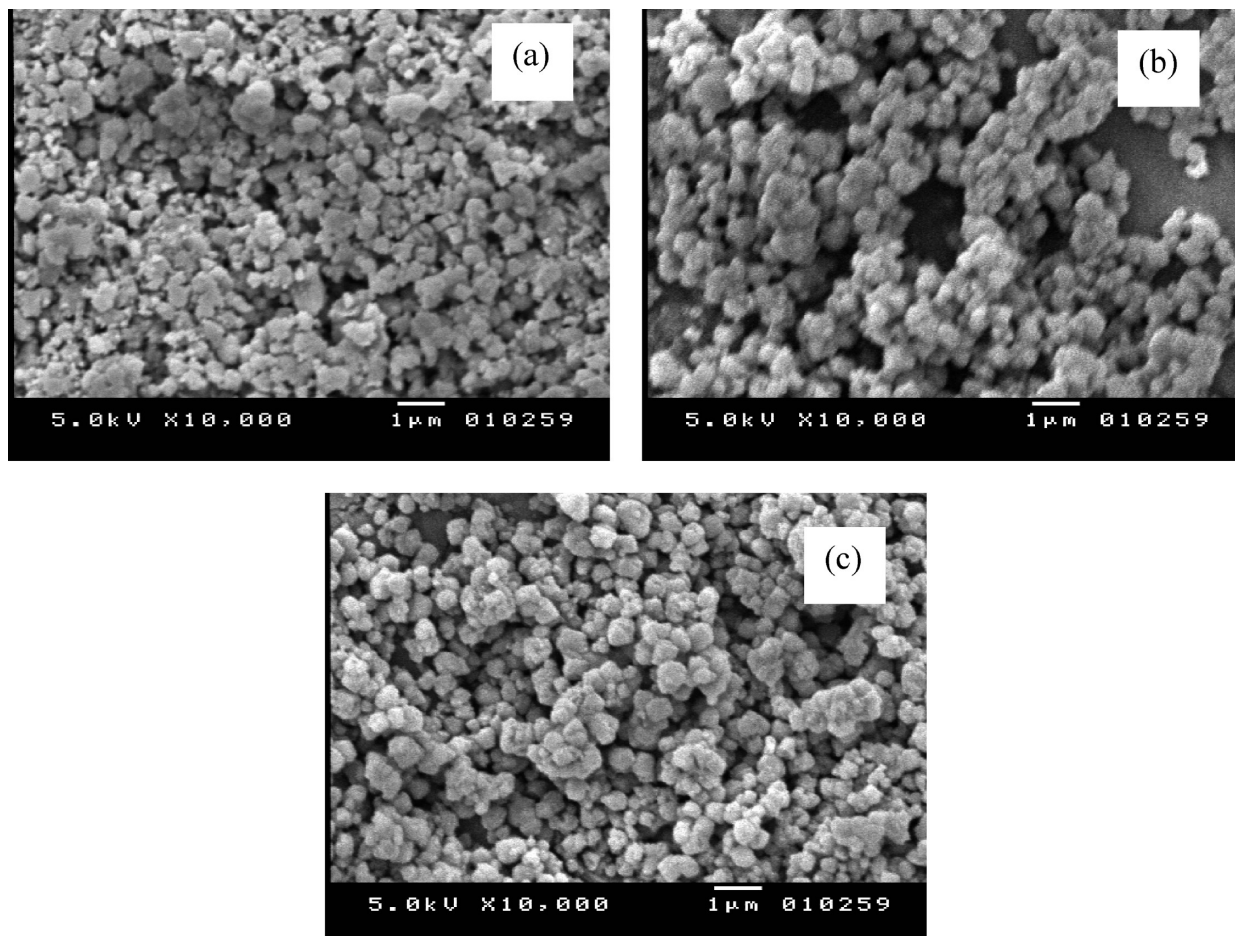


Figure 18. SEM micrographs of NaY zeolite from microwave synthesis using (a) center control (position V) without stirring, (b) periphery control (position IV) without stirring and center control (position V) with stirring. For the samples at the end of the plateau region on the crystallization curves.

TABLE 7: Particle Sizes and Numbers of NaY from Crystallization Using Different Positions in the Reactor to Control the Heating, with and without Stirring for the Samples at the End of the Plateau Region on the Crystallization Curves

controlled temperature	yield (g)	particle size ^a (μm)	estimated number of particles ^b × 10 ¹²
center middle (V), no stirring	10.28	0.40 ± 0.13	237
periphery middle (IV), no stirring	10.45	0.49 ± 0.12	131
center middle (V), with stirring	10.13	0.45 ± 0.12	164

^a Statistical size distribution based on 96 crystals. ^b Assuming spherical particles. Density⁴⁹ of 1.29 g cm⁻³.

continuous power delivery at the same average power. The penetration depth of water increases with an increase in temperature. This leads to a reduction in the amount of absorbed microwaves and thus a reduced heating rate. The absorbed microwave power was found to follow a linear function of temperature with average constant values of 17.7 and -0.16 W/K for continuous power delivery and 20.2 and -0.12 W/K for pulsed power delivery at (1 s on/2 s off). Although the proposed thermal model is simple, it shows the importance of considering the temperature-dependent dielectric properties and the knowledge of the E-field distribution within the dielectric media heated by microwaves to fully characterize its thermal interactions with microwaves.

Silicalite, SAPO-11, and NaY zeolite precursor solutions were used to demonstrate the temperature gradients in a 40 mm ID vessel, using five fiber-optic temperature probes. These temperature profiles were compared to that measured for water at a set point of 60 °C at the center of the solution. Water, silicalite, and SAPO-11 precursors show only a small temperature gradient and overheating due to the relatively large penetration depth.

In comparison, NaY precursor solution exhibits the greatest temperature gradients and overheating due to the relatively small penetration depth (2.6 mm at 25 °C and 2.45 GHz). Controlling the temperature at the periphery (position IV) significantly reduced the overheating (12 °C compared to 50 °C, with control at the center (V) and a 95 °C set point). Similar reduction in overheating was produced using stirring of the precursor solution.

The crystallization curves for NaY at 95 °C under center (position V) and periphery (position IV) temperature control were determined by reacting precursor material for different times and characterization with X-ray diffraction and SEM. It was found that center control (position V) leads to an enhanced reaction rate via nucleating the zeolite earlier, as compared to the periphery control (position IV). If stirring was used with center temperature control, the crystallization curve shifts toward that determined for periphery control, indicating that nonuniform temperature distribution enhances this synthesis. Furthermore, Ostwald ripening was found to be a possible process for NaY synthesis under these conditions.

Overheating is a significant effect, particularly for dielectric media with small penetration depths compared to the reaction vessel diameter. It accounts partially but not fully for the significant rate enhancement observed for many zeolite syntheses. Nonthermal effects such as microscopic and/or interfacial temperature gradients may also occur, giving rise to the rate enhancements observed.¹⁶

Finally, this study demonstrates the importance of overheating effects on microwave zeolite syntheses, which can be utilized through microwave reaction engineering parameters such as reactor geometry, applicator type (multimode vs monomode), microwave frequency, and microwave power delivery (pulsed vs continuous) to further enhance the synthesis rate. Further work on the effect of the microwave power delivery mode on zeolite synthesis is in progress.⁵⁵

Acknowledgment. The authors would like to thank the NSF under NIRT grant CTS-0304217 (Glenn Schrader) for funding this project. We also would like to thank Karl Hammond for the LabVIEW programming.

Supporting Information Available: Figure showing the dependence of the dielectric loss (ϵ''), dielectric permittivity (ϵ'), and penetration depth (δ_s) of water on the temperature and frequency. This material is available free of charge via the Internet at <http://pubs.acs.org>.

References and Notes

- (1) de la Hoz, A.; Diaz-Ortiz, A.; Moreno, A. *Chem. Soc. Rev.* **2005**, *34*, 164.
- (2) Kappe, C. O. *Angew. Chem., Int. Ed.* **2004**, *43*, 6250.
- (3) Cundy, C. S. *Collect. Czech. Chem. Commun.* **1998**, *63*, 1699.
- (4) Tompsett, G. A.; Conner, W. C.; Yngvesson, K. S. *ChemPhysChem* **2006**, *7*, 296.
- (5) Clark, D.; Folz, D. *Adv. Sci. Technol. (Faenza, Italy)* **2003**, *31*, 367.
- (6) Bogdal, D. Modern Polymeric Materials for Environmental Applications, International Seminar, 1st, Krakow, Poland, Dec. 16–18, 2004; Vol. 1, p 173.
- (7) Strauss, C. R.; Trainor, R. W. *Aust. J. Chem.* **1995**, *48*, 1665.
- (8) Immediate Energy Savings via: Microwave Usage in Major Materials Technologies. National Academy of Engineering - Northeastern Regional Meeting, 2006.
- (9) Chemat, F.; Pouix, M.; Di Martino, J. L.; Berlan, J. *Chem. Eng. Technol.* **1996**, *19*, 420.
- (10) Strauss, C. R. *Microwaves Org. Synth.* **2002**, *35*.
- (11) Park, S.-E.; Kim, D. S.; Chang, J.-S.; Kim, J.-M. Continuous process and apparatus for preparing inorganic materials employing microwave. *U.S. Pat. Appl. Publ. 2001054549* (Korea Research Institute of Chemical Technology, S. Korea). US, 2001; p 11.
- (12) Conner, W. C.; Tompsett, G. *J. Phys. Chem. B* **2008**, *112*, 2110.
- (13) Gharibeh, M.; Tompsett, G. A.; Conner, W. C. *Top. Catal.* **2008**, *49*, 157.
- (14) Choi, K.; Tompsett, G. A.; Conner, W. C. *Green Chem.* **2008**, *10*, 1313.
- (15) Conner, W. C.; Tompsett, G.; Lee, K.-H.; Yngvesson, K. S. *J. Phys. Chem. B* **2004**, *108*, 13913.
- (16) Blanco, C.; Auerbach, S. *J. Phys. Chem. B* **2003**, *107*, 2490.
- (17) Herrero, M.; Kremsner, J.; Kappe, C. O. *J. Org. Chem.* **2008**, *73*, 36.
- (18) Herrmann, R.; Scharf, O.; Schwieger, W. *Stud. Surf. Sci. Catal.* **2004**, *154A*, 155.
- (19) Bond, G.; Moyes, R. B.; Pollington, S. D.; Whan, D. A. *Chem. Ind. (London)* **1991**, 686.
- (20) Scherlen, R. Ph.D. Thesis, University of Karlsruhe, 2002.
- (21) Nuchter, M.; Muller, U.; Ondruschka, B.; Tied, A.; Lautenschlager, W. *Chem. Ing. Tech.* **2002**, *74*, 910.
- (22) Nuchter, M.; Ondruschka, B.; Bonrath, W.; Gum, A. *Green Chem.* **2004**, *6*, 128.
- (23) Darby, G.; Clark, D. E.; Di Fiore, R.; Folz, D.; Schulz, R.; Boonyapiwat, A.; Roth, D. *Ceram. Trans.* **1995**, *59*, 515.
- (24) Mullin, J.; Bows, J. *Food Addit. Contam.* **1993**, *10*, 663.
- (25) Degamber, B.; Fernando, G. F. *J. Appl. Polym. Sci.* **2003**, *89*, 3868.
- (26) Abtal, E.; Lallement, M.; Bertrand, G.; Roudergues, N. *Calorim. Anal. Therm.* **1984**, *15*, 220.
- (27) Geodakyan, K. T.; Kiselev, A. V.; Lygin, V. I. *Zh. Fiz. Khim.* **1967**, *41*, 457.
- (28) Bond, G.; Moyes, R. B.; Pollington, S. D.; Whan, D. A. *Meas. Sci. Technol.* **1991**, *2*, 571.
- (29) Thompson, K.; Booske, J. H.; Cooper, R. F.; Gianchandani, Y. B.; Ge, S. *Ceram. Trans.* **2001**, *111*, 391.
- (30) Pert, E.; Carmel, Y.; Birnboim, A.; Olorunyolemi, T.; Gershon, D.; Calame, J.; Lloyd, I. K.; Wilson, O. C., Jr. *J. Am. Ceram. Soc.* **2001**, *84*, 1981.
- (31) Ravindran, M.; Monsef-Mirzai, P.; Maund, J. K.; McWhinnie, W. R.; Burchill, P. *J. Therm. Anal.* **1995**, *44*, 25.
- (32) McSherry, M.; Fitzpatrick, C.; Lewis, E. *Proc. SPIE-Int. Soc. Opt. Eng.* **2005**, *5826*, 654.
- (33) Finegan, T.; Laibinis, P.; Hatton, T. *AIChE J.* **2006**, *52*, 2727.
- (34) Nott, K. P.; Hall, L. D.; Bows, J. R.; Hale, M.; Patrick, M. L. *Int. J. Food Sci. Technol.* **1999**, *34*, 305.
- (35) Nott, K. P.; Hall, L. D. *Int. J. Food Sci. Technol.* **2005**, *40*, 723.
- (36) Vallee, S.; Conner, W. C. *J. Phys. Chem. B* **2006**, *110*, 15459.
- (37) Panzarella, B.; Tompsett, G.; Conner William, C.; Jones, K. *ChemPhysChem* **2007**, *8*, 357.
- (38) Li, Y.; Yang, W. *J. Membr. Sci.* **2008**, *316*, 3.
- (39) Lok, B. M.; Messina, C. A.; Patton, R. L.; Gajek, R. T.; Cannan, T. R.; Flanigen, E. M. Crystalline silicoaluminophosphates, Union Carbide Corp., 1984; Vol. U.S. Patent 4440871.
- (40) Xomeritakis, G.; Nair, S.; Tsapatsis, M. *Microporous Mesoporous Mater.* **2000**, *38*, 61.
- (41) Gharibeh, M.; Tompsett, G.; Yngvesson, K. S.; Conner, W. C. *ChemPhysChem* **2008**, *9*, 2580.
- (42) Culfa, A.; Sand, L. B. *Adv. Chem. Ser.* **1973**, *121* (Mol. Sieves, Int. Conf., 3rd), 140.
- (43) Gizdavic-Nikolaidis, M.; Adnadjevic, B. *Sci. Sintering* **2001**, *33*, 189.
- (44) Grizzetti, R.; Artioli, G. *Microporous Mesoporous Mater.* **2002**, *53*, 105.
- (45) Metaxas, A. C.; Meredith, R. J. *Industrial Microwave Heating*; Peter Peregrinus, Ltd.: London, 1983.
- (46) English, N. J.; MacElroy, J. M. D. *J. Chem. Phys.* **2003**, *118*, 1589.
- (47) Barthel, J.; Buchner, R. *Pure Appl. Chem.* **1991**, *63*, 1473.
- (48) Panzarella, B.; Tompsett, G. A.; Yngvesson, K. S.; Conner, W. C. *J. Phys. Chem. B* **2007**, *111*, 12657.
- (49) Szostak, R. *Handbook of Molecular Sieves*; Van Nostrand Reinhold: New York, 1992.
- (50) Brar, T.; France, P.; Smirniotis, P. G. *Ind. Eng. Chem. Res.* **2001**, *40*, 1133.
- (51) Hadan, M.; Fischer, F. *Cryst. Res. Technol.* **1992**, *27*, 343.
- (52) Mintova, S.; Fieres, B.; Bein, T. *Stud. Surf. Sci. Catal.* **2002**, *142*, 223.
- (53) Jorge, M.; Auerbach, S.; Monson, P. *Mol. Phys.* **2006**, *104*, 3513–3522.
- (54) Rimer, J. D.; Trofymuk, O.; Navrotsky, A.; Lobo, R. F.; Vlachos, D. G. *Chem. Mater.* **2007**, *19*, 4189.
- (55) Gharibeh, M.; Tompsett, G. A.; Conner, W. C. *J. Phys. Chem. B* **2009**, in press.

JP900394U